The Unimoment Method and a Meshless Local Boundary Integral Equation (LBIE) Approach in 2D Electromagnetic Wave Scattering

Williams L. Nicomedes, Renato C. Mesquita*, and Fernando J. S. Moreira
Dept. of Electronics Engineering and *Dept. of Electrical Engineering
Federal University of Minas Gerais (UFMG), Belo Horizonte, Brazil
wlnicomedes@yahoo.com.br; renato@ufmg.br; fernandomoreira@ufmg.br

***Abstract*—In this work, we solve the scattering problem of a plane wave by a dielectric cylinder through the Unimoment Method, where a new approach was taken when solving the interior problem: a meshless method based on local boundary integral equations (LBIE). Traditionally, the interior problem is attacked through the Finite Element Method, because one gets sparse matrices. But as in FEM, a meshless LBIE approach also provides sparse matrices, without the drawback of constructing a grid. We develop the formalism and illustrate the application of the aforementioned method to the scattering by a dielectric circular cylinder, a problem which is known to possess analytical solution.**

Keywords-Unimoment, Meshless, LBIE, RPIM, Scattering

I. INTRODUCTION

The unimoment method was devised by K. Mei [1] as a hybrid method intended to solve the scattering fields by dielectric bodies in unbounded domains. In two-dimensional analyses, the main idea is to set up a mathematical circle around the scatterer cross-section, dividing the problem into two ones: an interior and an exterior. The fields in the exterior region are expressed as a sum of Hankel functions, representing outward-travelling waves. The fields in the interior, by their turn, are given by a sum of solutions obtained through some numerical method, usually FEM [1]. Once these interior solutions are formed, one imposes the continuity of the fields and their normal derivatives along the mathematical circle, matching both problems at this boundary. The solutions of the interior and the exterior problems may then be expressed as sum of modal solutions, with Hankel functions in the exterior and numerical ones in the interior.

In this work, we take a different approach: a meshless method. Meshless methods are relatively new; only recently they have been applied as a tool for numerical solutions in engineering [2], [3]. The family of meshless methods is intended to be a substitute for the Finite Element Method (FEM). As it is well known, FEM requires a mesh, or a grid with connectivity between the elements, which sometimes demonstrates to be a strong shortcoming. Meshless methods, otherwise, require no mesh; nodes are simply spread over the domain and no connectivity between them is demanded. This makes them very attractive because they work on the same grounds as FEM in what concerns local interactions (producing sparse matrices) and have no need for any mesh.

In this work, we use a particular method, the LBIE method together with a meshless discretization approach, in order to get a purely local method, also known as Meshless Local Petrov Galerkin 4 (MLPG 4, where 4 stands for the type of the test function employed) [2]. This local method is applied to the scattering problem of a TM plane wave by a homogeneous dielectric cylinder. We could then compare the numerical results with the analytical solution, observing an excellent agreement between them.

II. THE UNIMOMENT METHOD

A. Overview

Given a scatterer with its characteristic cross section (shaded region in Fig. 1), we set up a circumference Γ surrounding it, thus dividing the space in two domains: the exterior (region I) and the interior (region II). The scatterer is to be entirely located inside region II, as in Fig. 1. For a TM^z incident wave, in which the electric field has only the z-component, we can write (in polar coordinates ρ and φ):

$$E_z^I(\rho,\varphi) = E_z^{inc}(\rho,\varphi) + E_z^s(\rho,\varphi) \tag{1}$$

for the total field in region I, as a sum of the incident and scattered fields. The scattered field E_z^s is expressed as an infinite sum of Hankel functions of the second type; but only the first N will be taken into account:

$$E_z^s(\rho,\varphi) = \sum_{n=-N}^{N} A_n H_n^{(2)}(k\rho) e^{jn\varphi} \tag{2}$$

where the coefficients A_n remain to be evaluated. The wavenumber $k = 2\pi/\lambda$ is related to the exterior medium. The total field in region II is expressed by a sum of numerical basis functions:

$$E_z^{II}(\rho,\varphi) = \sum_{n=-N}^{N} B_n \psi_n(\rho,\varphi) \tag{3}$$

where B_n are coefficients to be determined and ψ_n are the numerical basis functions.

The next step is to impose the continuity of the total field along both sides of the mathematical boundary Γ.

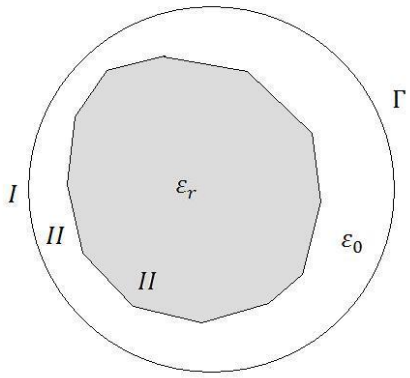

Figure. 1 The circular boundary Γ divides the domain in two regions: exterior (I) and interior (II). The solutions in both regions are to be matched in Γ. The shaded area represents the cylinder cross-section.

The next step is to impose the continuity of the total field along both sides of the mathematical boundary Γ. Supposing this boundary to be located at a radius $\rho = a$, we arrive at two conditions:

$$E_z^{inc}(\vec{\rho})\big|_{\rho=a} + E_z^{s}(\vec{\rho})|_{\rho=a} = E_z^{II}(\vec{\rho})|_{\rho=a} \tag{4}$$

$$\left.\frac{\partial E_z^{inc}(\vec{\rho})}{\partial n}\right|_{\rho=a} + \left.\frac{\partial E_z^{s}(\vec{\rho})}{\partial n}\right|_{\rho=a} = \left.\frac{\partial E_z^{II}(\vec{\rho})}{\partial n}\right|_{\rho=a} \tag{5}$$

B. Numerical basis functions for the interior problem

From the above expressions one sees that the infinite sum was replaced by a finite sum, with terms whose indices range from $-N$ to N, and there are no clue about the form of the numerical solutions ψ_n. They will then assumed to be solutions to the homogeneous Helmholtz equation:

$$\nabla^2\psi_n(\vec{\rho}) + k^2\varepsilon_r(\vec{\rho})\psi_n = 0 \tag{6}$$

where the relative permittivity ε_r can be a function of position, $\varepsilon_r(\vec{\rho})$. Now comes one of the remarkable features of the method: for each n, the Helmholtz equation (6) shall be subject to a characteristic Dirichlet condition enforced at the boundary $\rho = a$. A linearly independent set of Dirichlet conditions is set up, i.e., for each n, one chooses the associated condition:

$$\left\{e^{-jN\varphi}, e^{-j(N-1)\varphi}, \dots, 1, \dots, e^{jn\varphi}, \dots, e^{j(N-1)\varphi}, e^{jN\varphi}\right\} \tag{7}$$

So, for a given n, taking (6) together with the associated Dirichlet condition $e^{jn\varphi}$ one finds the interior solution ψ_n throughout the interior domain (region II). After doing that for n ranging form $-N$ to N, the whole set of 'modal' interior solutions is formed. The equations (4) and (5) are then taken into account; when they are finally solved, the coefficients A_n and B_n of the field expansions are determined. The total interior field is thus given by (3).

C. Finding the coefficients of the modal expansions

In order to enforce (4) and (5) at the boundary $\rho = a$, we multiply these equations by a test function and integrate along the boundary contour. Taking the test function as $e^{-jm\varphi}$, where m ranges from $-N$ to N, and keeping in mind that the numerical basis functions ψ_n vary as $e^{jn\varphi}$ at the boundary, we arrive at two expressions relating the coefficients A_n and B_n. After some manipulations, these expressions can be put in matrix form:

$$\begin{bmatrix} \boldsymbol{M_1} & \boldsymbol{M_2} \\ \boldsymbol{M_3} & \boldsymbol{M_4} \end{bmatrix} \begin{bmatrix} \boldsymbol{b} \\ \boldsymbol{a} \end{bmatrix} = \begin{bmatrix} \boldsymbol{f_1} \\ \boldsymbol{f_2} \end{bmatrix} \tag{8}$$

where each of the submatrices $\boldsymbol{M}$ has the size $(2N+1)$, and $\boldsymbol{b}, \boldsymbol{a}, \boldsymbol{f}_1$ and $\boldsymbol{f_2}$ are vectors whose size is also $(2N+1)$. The total system then has the size $(4N+2)$. $\boldsymbol{M}_1, \boldsymbol{M_2}$ and $\boldsymbol{M}_4$ are diagonal matrices. Their elements are given by

$$[\boldsymbol{M_1}]_{mm} = 2\pi \tag{9}$$

$$[\boldsymbol{M_2}]_{mm} = -2\pi H_m^{(2)}(ka) \tag{10}$$

$$[\boldsymbol{M_4}]_{mm} = -2\pi \left.\frac{\partial H_m^{(2)}(k\rho)}{\partial n}\right|_{\rho=a} \tag{11}$$

$\boldsymbol{M}_3$ is a full matrix with elements:

$$[\boldsymbol{M_3}]_{mn} = \int_0^{2\pi} \left.\frac{\partial \psi_n}{\partial n}\right|_{\rho=a} e^{-jm\varphi}\, d\varphi \tag{12}$$

The vectors $\boldsymbol{f}_1$ and $\boldsymbol{f_2}$ have components:

$$[\boldsymbol{f}_1]_m = \int_0^{2\pi} E_z^{inc}\big|_{\rho=a}\, e^{-jm\varphi}\, d\varphi \tag{13}$$

$$[\boldsymbol{f}_2]_m = \int_0^{2\pi} \left.\frac{\partial E_z^{inc}}{\partial n}\right|_{\rho=a} e^{-jm\varphi}\, d\varphi \tag{14}$$

The coefficients of the modal expansions (2) and (3) are given by the vectors $\boldsymbol{a^T} = [A_{-N}, \dots, A_N]$ and $\boldsymbol{b^T} = [B_{-N}, \dots, B_N]$, solutions to (8).

III. THE LOCAL BOUNDARY INTEGRAL EQUATION

As already stated, the interior solutions ψ_n ,which are solutions of (6) and (7), are usually solved through FEM [1]. We now proceed to show a different approach: the LBIE.

Considering a plane domain Ω (the interior region II, Fig. 2) with boundary Γ, we seek for the solutions of the Helmholtz equation (6) inside this domain. Given a point $\vec{x}_i$ inside the domain (for example, the point X in Fig. 2) we then take a test function u centered at $\vec{x}_i$, so that it satisfies (δ is the Dirac delta function)

$$\nabla^2 u = -\delta(\vec{x} - \vec{x}_i) \tag{15}$$

Its solution is known to be:

$$u(\vec{x}; \vec{x}_i) = \frac{1}{2\pi} ln\left(\frac{1}{r}\right) \tag{16}$$

where $r = \sqrt{(x-x_i)^2 + (y-y_i)^2}$ and (x_i, y_i) are the coordinates of point $\vec{x}_i$ .Applying to ψ_n and u the second Green's identity, we get:

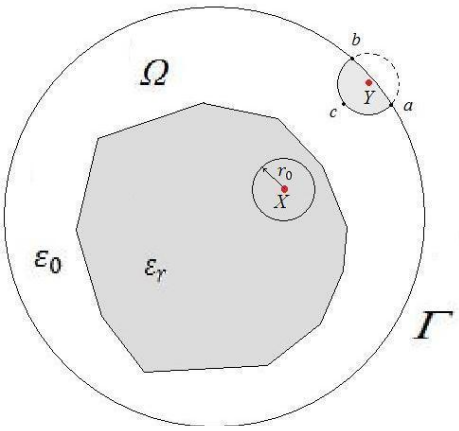

Figure 2. The problem domain Ω and the global boundary Γ. The irregular shaded area is the scatterer cross-section, characterized by a relative permittivity ε_r. X and Y are points at which E_z shall be calculated. X is an interior point, with a circular subdomain of radius r_0. Although Y is also an interior point, its subdomain intersects the global boundary, resulting in a noncircular local boundary (shaded area).

$$-\alpha(\vec{x}_i)\psi_n(\vec{x}_i) + \iint_\Omega k^2\varepsilon_r u\psi_n dS = \oint_\Gamma \psi_n \frac{\partial u}{\partial n} dl - \oint_\Gamma u \frac{\partial \psi_n}{\partial n} dl \qquad (17)$$

The surface integral is to be evaluated at the interior domain Ω (region II) and the line integral at the global boundary Γ. The factor α arises in the integration of the delta function. It is equal to 1 for every $\vec{x}_i$ inside the domain; however, if $\vec{x}_i$ is exactly at the global boundary Γ, then α is proportional to the internal angle at $\vec{x}_i$ (for example, were $\vec{x}_i$ to be located at the corner of a square, α would be $1/4$; were it to be located at a wedge with internal angle equal to θ radians, α would be $\theta/2\pi$). For a circular boundary, α is approximately equal to $1/2$. Because the line integrals are evaluated at the global boundary Γ, ψ_n and $\partial\psi_n/\partial n$ are respectively the Dirichlet and Neumann conditions prescribed at the global boundary Γ.

If, instead of integrating at the entire domain, we consider the integrations only at a local subdomain Ω_s (local boundary Γ_s) around the point $\vec{x}_i$ [2] (small circle around X at Fig.2), expression (17) still holds, but ψ_n and $\partial\psi_n/\partial n$ are no longer the known Dirichlet and Neumann conditions. So there are two unknowns at the local subdomain boundary, ψ_n and its normal derivative $\partial\psi_n/\partial n$. To avoid at least one of them, we arrange so that $\partial\psi_n/\partial n$ does not appear in (17), through the use of a slightly different test function u^* that goes to zero at the local boundary. If the subdomain is a circular one with radius r_0, then u^* is

$$u^* = u^*(\vec{x};\vec{x}_i) = \frac{1}{2\pi} ln\left(\frac{r_0}{r}\right) \qquad (18)$$

So, (17) becomes

$$-\alpha(\vec{x}_i)\psi_n(\vec{x}_i) + \iint_{\Omega_s} k^2\varepsilon_r u^*\psi_n dS = \oint_{\Gamma_s} \psi_n \frac{\partial u^*}{\partial n} dl - \oint_{\Gamma_s} u^* \frac{\partial \psi_n}{\partial n} dl \qquad (19)$$

The line integrals in (19) shall be evaluated at the local boundary, a circle located r_0 away from $\vec{x}_i$. For points whose local domains don't intersect the global boundary Γ (like X in Fig. 2), the last line integral in (19) does not need to be carried out. But for points like Y (Fig. 2), whose local domains are not circular, but a intersection between two circles, u^* is no longer zero in that portion that corresponds to the global boundary Γ (the dashed line is not a part of the local domain, only the shaded part). Taking the line integrals in (19), and considering their closed contour (local boundary) as a sum of two paths, one called *internal boundary* (ib), that is a line integral along the path acb and the other called *global boundary* (gb), that is a line integral along path ab, there follows:

$$-\alpha(\vec{x}_i)\psi_n(\vec{x}_i) + \iint_{\Omega_s} k^2\varepsilon_r u^*\psi_n dS = \int_{ib} \psi_n \frac{\partial u^*}{\partial n} dl + \int_{gb} \psi_n \frac{\partial u^*}{\partial n} dl - \int_{ib} u^* \frac{\partial \psi_n}{\partial n} dl - \int_{gb} u^* \frac{\partial \psi_n}{\partial n} dl \qquad (20)$$

The third line integral is zero, because it depends on u^* evaluated at a distance $r = r_0$ from $\vec{x}_i$. So we obtain, after some rearrangement:

$$\alpha(\vec{x}_i)\psi_n(\vec{x}_i) - \iint_{\Omega_s} k^2\varepsilon_r u^*\psi_n dS + \int_{ib} \psi_n \frac{\partial u^*}{\partial n} dl - \int_{gb} u^* \frac{\partial \psi_n}{\partial n} dl = -\int_{gb} \psi_n \frac{\partial u^*}{\partial n} dl \qquad (21)$$

This is the local integral equation (LBIE) that must be satisfied for every point $\vec{x}_i$ in the domain. For each n, one picks up the associated Dirichlet boundary condition in (7) and replaces ψ_n for $e^{jn\varphi}$ in the right side of (21). If $\vec{x}_i$ is an interior point whose local boundary does not intersect the global boundary (X in Fig. 2), there is no integration along a path like ab, and the terms which depend on gb are discarded.

IV. THE MESHLESS APPROACH

In order to get the numerical basis functions ψ_n, the next step is to apply a meshless discretization to solve (21). The meshless approach begins by spreading nodes over the domain of the problem to be solved (in this case, the interior region II). Nodes are simple points and to each one a *shape function* is associated. Each shape function has the property of being zero over the whole domain, except in the vicinity of the corresponding node. The vicinal region in which the shape function is different from zero is the node's *influence domain* [3]. The main difference between meshless methods and mesh-based methods (like FEM) is that the *element* concept is not present. The influence domains are arbitrary (the only

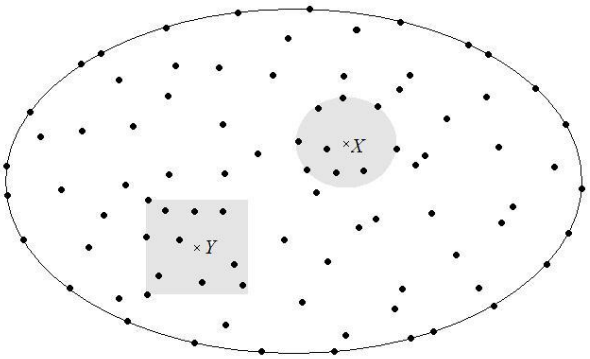

Figure 3. Nodes spread in a general domain. Those ones that influence points X and Y are shown as belonging to regions that surround these points (shaded regions).

restriction is that the set of influence domains must cover the entire domain) and can overlap. So, the nodes can be distributed arbitrarily without generating an element mesh.

For a given point (e.g. point $\vec{x} = X$ in Fig. 3), an unknown solution u is expressed as a sum of the contributions of those nodes that influence X, i.e. nodes that extend their influence domains onto X (they are depicted inside the circular shaded region):

$$u(\vec{x}) \sim u^h(\vec{x}) = \sum_{i=1}^{N} \phi_i(\vec{x})\hat{u}_i = \boldsymbol{\Phi}(\vec{x})\boldsymbol{u} \qquad (22)$$

where u^h is the approximated solution, N is the number of nodes whose influence domains include the point $\vec{x}$, each ϕ_i is the i-th node shape function evaluated at $\vec{x}$, and $\hat{u}_i$ is the associated nodal parameter.

Shape function construction

There are a number of schemes to build the shape functions. We have used the Radial Point Interpolation Method with Polynomial Reproduction (RPIM-PR) [3]. This choice is suitable because the shape functions obtained through RPIM-PR satisfy the Kronecker Delta property, i.e., they are equal to 1 at a node and equal to zero at the other nodes, a desirable feature when imposing Dirichlet conditions. In the RPIM-PR u^h in a point $\vec{x}$ is expressed as:

$$u^h(\vec{x}) = \sum_{i=1}^{N} R_i(\vec{x})a_i + \sum_{j=1}^{m} p_j(\vec{x})b_j = \boldsymbol{R}^T\boldsymbol{a} + \boldsymbol{p}^T\boldsymbol{b} \qquad (23)$$

where N stands for the number of nodes that influence point $\vec{x}$. Each radial basis function R_i, as its name indicates, is a function of the distance between point $\vec{x}$ and the i-node which exerts influence onto $\vec{x}$. Among various schemes, we have chosen R_i to be a multiquadrics [3]:

$$R_i(\vec{x}) = R_i(x, y) = [(x - x_i)^2 + (y - y_i)^2 + C^2]^q \qquad (24)$$

(x_i, y_i) is the position of node i, and C and q are shape parameters. Besides the radial basis functions R_i, there are still m polynomial terms. Taking only the polynomial terms which build a linear basis, we have chosen each $p_j(\vec{x})$ to be a linear term, i.e. $\boldsymbol{p}^T(\vec{x}) = [1, x, y]$. $\boldsymbol{a}^T = [a_1, \dots, a_N]$ and $\boldsymbol{b}^T = [b_1, \dots, b_m]$ are coefficients that remain to be determined.

To determine $\boldsymbol{a}$ and $\boldsymbol{b}$, one enforces N interpolations passing through each of all N nodes which influence point $\vec{x}$. For a given k, where $1 \ll k \ll N$, the k-interpolation has the form:

$$\hat{u}_k = u(x_k, y_k) = \sum_{i=1}^{N} R_i(x_k, y_k)\, a_i + \sum_{j=1}^{m} p_j(x_k, y_k) b_j \qquad (25)$$

Or in matrix form

$$\boldsymbol{u} = \boldsymbol{R_Q}\boldsymbol{a} + \boldsymbol{P_m}\boldsymbol{b} \qquad (26)$$

where $\boldsymbol{u}$ is a vector with the N nodal parameters, $\boldsymbol{R_Q}$ is a $N \times N$ matrix:

$$\boldsymbol{R_Q} = \begin{bmatrix} R_1(\vec{x}_1) & \cdots & R_N(\vec{x}_1) \\ \vdots & \ddots & \vdots \\ R_1(\vec{x}_N) & \cdots & R_N(\vec{x}_N) \end{bmatrix} \qquad (27)$$

and P_m is a $N \times m$ matrix:

$$\boldsymbol{P_m} = \begin{bmatrix} p_1(\vec{x}_1) & \dots & p_m(\vec{x}_1) \\ \vdots & \ddots & \vdots \\ p_1(\vec{x}_N) & \dots & p_m(\vec{x}_N) \end{bmatrix} \qquad (28)$$

Only $\boldsymbol{R_Q}$ and $\boldsymbol{P_m}$ don't provide enough information to uniquely solve (26). Another constraint is imposed [3]

$$\sum_{i=1}^{N} p_j(x_i, y_i)\, a_i = 0 \quad j = 1, \dots, m \qquad (29)$$

or :

$$\boldsymbol{P_m^T}\boldsymbol{a} = 0 \qquad (30)$$

$\boldsymbol{a}$ and $\boldsymbol{b}$ can then be determined through the system:

$$\begin{bmatrix} \boldsymbol{R_Q} & \boldsymbol{P_m} \\ \boldsymbol{P_m^T} & \boldsymbol{0} \end{bmatrix} \begin{bmatrix} \boldsymbol{a} \\ \boldsymbol{b} \end{bmatrix} = \begin{bmatrix} \boldsymbol{u} \\ \boldsymbol{0} \end{bmatrix} \qquad (31)$$

Once vectors $\boldsymbol{a}$ and $\boldsymbol{b}$ are found, they are substituted back in (23). After some manipulation and comparing the result with (22) one arrives at an expression for the shape functions:

$$\boldsymbol{\Phi}(\vec{x}) = [\phi_1(\vec{x}), \dots, \phi_N(\vec{x})] = \boldsymbol{R^T}(\vec{x})\boldsymbol{S_a} + \boldsymbol{p^T}(\vec{x})\boldsymbol{S_b} \qquad (32)$$

where $\boldsymbol{S_a}$ and $\boldsymbol{S_b}$ are matrices given by:

$$\boldsymbol{S_b} = \left[\boldsymbol{P_m^T}\boldsymbol{R_Q^{-1}}\boldsymbol{P_m}\right]^{-1}\boldsymbol{P_m^T}\boldsymbol{R_Q^{-1}} \qquad (33)$$

$$\boldsymbol{S_a} = \boldsymbol{R_Q^{-1}} - \boldsymbol{R_Q^{-1}}\boldsymbol{P_m}\boldsymbol{S_b} \qquad (34)$$

So there is no analytical expression for the shape functions. They need to be calculated numerically. But one of its advantages is that the derivatives are readily available:

$$\left[\frac{\partial \phi_1}{\partial x}, \dots, \frac{\phi_N}{\partial x}\right] = \left[\frac{\partial R_1}{\partial x}, \dots, \frac{\partial R_N}{\partial x}\right]\boldsymbol{S_a} + \left[\frac{\partial p_1}{\partial x}, \dots, \frac{\partial p_m}{\partial x}\right]\boldsymbol{S_b} \qquad (35)$$

The same holds for the derivatives with respect to y.

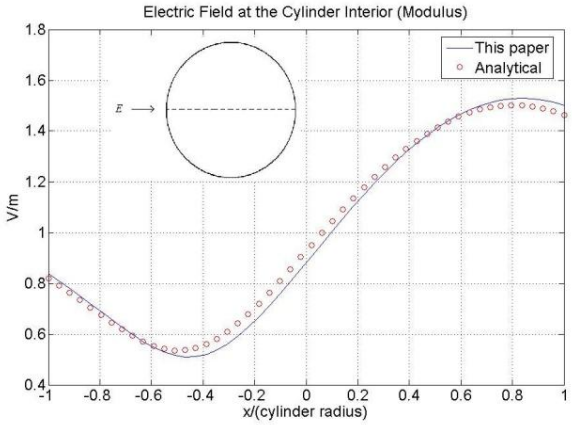

Figure 4. Electric field calculated along the dashed line (modulus). Dimension x is normalized with respect to the cylinder radius.

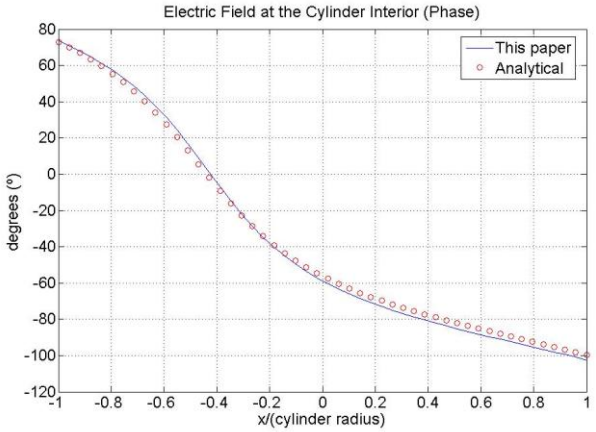

Figure 5. Electric field calculated along the dashed line (phase). Dimension x is normalized with respect to the cylinder radius.

V. DISCRETIZATION AND NUMERICAL IMPLEMENTATION

To obtain the numerical 'modal' solutions ψ_n, we proceed by spreading nodes over Ω (interior region II) and its global boundary Γ. Then, ψ_n at any given point $\vec{x}$ inside Ω (or at the boundary Γ) is expressed as a sum of shape functions associated to each node whose influence domain extends over $\vec{x}$:

$$\psi_n(\vec{x}) = \sum_{I=1}^{N} \phi_I(\vec{x})\hat{u}_I \tag{36}$$

where N is the number of nodes that influence point $\vec{x}$. To find the nodal parameters $\hat{u}_I$, we enforce the LBIE (21) at each node. The overall procedure is then:

First: Take each node and determine its local domain, verifying if it intersects the global boundary;

Second: Carry out the integrals described in (21). To each node $\vec{x}_i$, evaluate which other nodes influence its local domain.

Third: Assemble in a matrix the interactions between pairs of nodes and solve the resulting linear system.

Once the nodal parameters are found, the 'modal' solution ψ_n can be calculated everywhere in the domain through application of (36).

After all 'modal' solutions have been found, one has to evaluate the matrix entries in the unimoment system (8). The evaluation of the normal derivatives of ψ_n in the matrix $\boldsymbol{M_3}$ is straightforward, requiring just to find out which nodes influence a point and then applying (35) to obtain the rectangular derivatives. Remembering then that $\partial\psi_n/\partial n = \nabla\psi_n \cdot \hat{\boldsymbol{n}}$, where $\hat{\boldsymbol{n}}$ is the outward-pointing unit normal vector, there follows:

$$\frac{\partial\psi_n}{\partial n} = \sum_{i=1}^{N} \hat{u}_i \left[\frac{\partial\phi_i}{\partial x}\hat{\boldsymbol{x}} + \frac{\partial\phi_i}{\partial y}\hat{\boldsymbol{y}}\right] \cdot \hat{\boldsymbol{n}} \tag{37}$$

To verify the precision of the method, we have applied it to the scattering analysis of a plane wave by a dielectric circular cylinder, a problem which is known to possess analytical solution. The results obtained are precise, as illustrated by Figs. (4) and (5), which show the amplitude and phase for the scattering of a TM^z plane wave having unit amplitude by a cylinder with radius $\lambda/2\pi$ and relative permittivity $\varepsilon_r = 3$. Approximately 340 nodes have been spread over the domain Ω (although coarser results begin to appear when only 91 nodes are spread).

VI. CONCLUSION

In this work, we have solved the scattering problem of a plane wave by a dielectric cylinder through the unimoment method together with a meshless LBIE approach. The unimoment method has advantages over a pure FEM or a pure meshless LBIE formulation, because no radiation boundary conditions are required. Otherwise, it has the drawback of having to solve many Dirichlet problems, a feature absent in both aforementioned methods. In what regards the interior problem, the meshless LBIE has proven to be a good alternative to FEM. These two methods produce sparse matrices in calculating the interior solutions, but the meshless LBIE requires no mesh. A shortcoming is that the shape functions need to be calculated numerically, which could render the procedure costly.

REFERENCES

[1] S. K. Chang and K. K. Mei, "Application of the Unimoment Method to Electromagnetic Scattering of Dielectric Cylinders", IEEE Trans. Antennas Propagat., vol. AP-24, no 1, pp 35-42, Jan. 1976.

[2] S. N. Atluri and S. Shen, " The Meshless Local Petrov-Galerkin Method: A simple & less-costly alternative to the finite-element and boundary element methods", CMES, vol. 3, no 1, pp 11-51, 2002.

[3] G. Liu, Mesh Free Methods: Moving Beyond the Finite Element Method, CRC Press, 2002.